RSC Advances

PAPER

Cite this: *RSC Adv.*, 2023, **13**, 28008

Catalytic performance and antibacterial behaviour with molecular docking analysis of silver and polyacrylic acid doped graphene quantum dots†

Tahreem Aziz,[a] Muhammad Imran,[a] Ali Haider,[b] Anum Shahzadi,[c] Muhammad Zain Ul Abidin,[d] Anwar Ul-Hamid,[e]* Walid Nabgan,[f]* Mohammed M. Algaradah,[g] Ahmed M. Fouda[h] and Muhammad Ikram[d]*

Received 14th July 2023
Accepted 16th September 2023

DOI: 10.1039/d3ra04741e

rsc.li/rsc-advances

In this research, a fixed concentration (3 wt%) of Ag/PAA and PAA/Ag doped graphene quantum dots (GQDs) were synthesized using the co-precipitation technique. A variety of characterization techniques were employed to synthesize samples to investigate their optical, morphological, structural, and compositional analyses, antimicrobial efficacy, and dye degradation potential with molecular docking analysis. GQDs have high solubility, narrow band gaps, and are suitable for electron acceptors and donors but show less adsorption and catalytic behavior. Incorporating polyacrylic acid (PAA) into GQDs increases the catalytic and antibacterial activities due to the carboxylic group (–COOH). Furthermore, introducing silver (Ag) increased the degradation of dye and microbes as it had a high surface-to-volume ratio. In addition, molecular docking studies were used to decipher the mechanism underlying the bactericidal action of silver and polyacrylic acid-doped graphene quantum dots and revealed inhibition of β-lactamase and DNA gyrase.

1. Introduction

Urban sprawl and rapid industry growth have exacerbated freshwater scarcity.[1] Industries like paper, textiles, food, leather, and plastic release harmful chemicals, synthetic dyes, heavy metals, and other organic pollutants into the water reservoir, leading to water contamination.[2] 7×10^5 tons of dyes originate from textile industries per year, such as safranin dye, methylene blue (MB), methyl orange, methyl red, and rhodamine B dye (RhB). RhB ($C_{28}H_{31}N_2O_3Cl$) belongs to the family of xanthene dyes, released directly or indirectly into water resources, threatening human beings with various diseases like cancer, skin irritation, renal failure, respiratory disorders, eye burns, and hepatic dysfunction.[3–5] Moreover, effluent water contains infective agents, including algae, viruses, bacteria, and other microorganisms.[6] The most common multidrug resistance (MDR) bacterium, *Escherichia coli* (*E. coli*), is responsible for nosocomial infection[7] and causes 2.5 million deaths of children every year from diarrhea.[8] Degrading organic pollutants and removing metallic ions or pathogens from wastewater is imperative for water purification. Several techniques have been manifested for treating contaminated water, including ion exchange, membrane filtration, adsorption/precipitation, photo-catalysis, catalysis, electrochemical, and enzymatic decomposition.[9–11] Among these, catalysis in the presence of a nano-material has gained much attention attributed to its environmentally friendly nature, cost-effectiveness, and excellent efficiency in water purification.[12] Nano-materials have proven to be a practical field for wastewater remediation due to their different physical and chemical properties, like shape, size, and surface area to volume ratio, which play a productive role in the purification of contaminated water.[13–15] Nano-materials (ZnO, TiO_2, CeO_2, CdS, and La_2O_3) can remove heavy metal ions, toxic dyes, and other infectious bacteria.[16,17] Among these, semiconductor nano-materials are successfully utilized for catalytic dye degradation even with a sufficient band gap.[18] A two-dimensional (2D) gapless semiconductor graphene discovered in 2004 became of particular interest to researchers because of having excellent electrical properties, high surface

[a]*Department of Chemistry, Government College University, Faisalabad, Pakpattan Road, Sahiwal, Punjab, 57000, Pakistan*

[b]*Department of Clinical Sciences, Faculty of Veterinary and Animal Sciences, Muhammad Nawaz Shareef University of Agriculture, Multan 66000, Punjab, Pakistan*

[c]*Faculty of Pharmacy, The University of Lahore, Lahore, 54000, Pakistan*

[d]*Solar Cell Applications Research Lab, Department of Physics, Government College University Lahore, Lahore 54000, Punjab, Pakistan. E-mail: dr.muhammadikram@gcu.edu.pk*

[e]*Core Research Facilities, King Fahd University of Petroleum & Minerals, Dhahran, 31261, Saudi Arabia*

[f]*Departament d'Enginyeria Química, Universitat Rovira i Virgili, Av Països Catalans 26, 43007, Tarragona, Spain. E-mail: walid.nabgan@urv.cat*

[g]*Chemistry Department, King Khalid Military Academy, Riyadh 11495, Saudi Arabia*

[h]*Chemistry Department, Faculty of Science, King Khalid University, Abha 61413, Saudi Arabia*

† Electronic supplementary information (ESI) available. See DOI: https://doi.org/10.1039/d3ra04741e

area (2630 m^2 g^{-1}), less toxicity, and high thermal conductivity (5000 W m^{-1} K^{-1}).[19,20] Graphene has been intensively used as a catalyst for degrading pollutants and has wide applications in sensors, solar cells, and batteries.[21,22] Among graphene nanostructures, thin layers GQDs (100 nm) have gained a lot of attention[23,24] for characteristics like photoluminescence, high stability, narrow bandgap energy, good electron acceptors, and donors.[25,26] But its applications are limited due to low solubility, poor luminescence,[27] and inferior catalytic. To enhance the catalytic activity, doping with metals, nonmetals, and polymers has been suggested. Incorporating an organic polymer such as PAA increases the catalytic and antibacterial activities due to the presence of a carboxylic group (–COOH). It is a protective capping agent, capturing heavy metals from polluted water.[28] The doping of inorganic metals such as Ag increased the degradation of dye and microbes because of the high surface-to-volume ratio.[29] The combination of Ag and PAA dopants provides a large surface area for the adsorption of pollutants.[30] Two approaches (top-down and bottom-up) are applied to the synthesis GQDs in top-down method focuses on breaking the precursors such as carbon fibres, graphene sheets, and other carbonaceous compounds. In contrast, the bottom-up approach involves assembling basic units into nano-material.[31] In the present study, a simple bottom-up method involving pyrolysis of glucose was used to prepare GQDs from the organic precursor to investigate the catalytic efficacy against RhB degradation and bactericidal potency for *E. coli*. This research contributes to discovering multifunctional, defensible, eco-friendly, and economic catalysts for maintaining water standards by reducing toxic products and blocking bacterial cell proliferation.

2. Experimental

2.1 Materials and reagents

Glucose ($C_6H_{12}O_6$, 99.5%), ammonia solution (33%), polyacrylic acid $(C_3H_4O_2)_n$, $AgNO_3$, 99.8%, and HCl, 37% were acquired from Sigma Aldrich.

2.1.1 Synthesis of GQDs, PAA, and Ag-doped GQDs. To synthesize GQDs, pyrolysis of glucose was performed. Initially, 4 g of glucose was heated at 260 °C to liquefy, and after 20 min, the yellow color shifted to orange. Subsequently, NH_3 solution (12.5%) was incorporated dropwise to liquefy glucose under continuous stirring at 70 °C for 3 h to remove the ammonia odor. To obtain neutral pH, HCl was added, and the mixture was stirred magnetically at 150 °C for 12 h and crushed to get a fine powder, as shown in Fig. 1.

2.1.2 Synthesis of Ag/PAA-doped GQDs. For doping, fixed amounts of (3 wt%) Ag and PAA were added into the prepared GQDs solution at pH around 12 under vigorous stirring (Fig. 1). The mixture was heated for two hours at 100 °C, centrifuged twice at 7000 rpm for 7 min, then washed with DI water to obtain precipitates. Ultimately, the residues were dried overnight at 100 °C to obtain a refined powder of Ag/PAA-GQDs.

2.1.3 Synthesis of PAA/Ag-doped GQDs. Fixed amounts of (3 wt%) PAA and Ag were introduced into the synthesized GQDs solution at pH ~ 12 under continuous stirring for the required nanocomposite (Fig. 1). To obtain precipitates; the mixture was heated for 2 h at 100 °C, centrifuged two times at 7000 rpm for 7 min and then cleaned with DI water. Finally, residues were dried overnight at 100 °C to obtain a fine powder of PAA/Ag-GQDs.

2.2 Instrumental measurements

2.2.1 Catalytic activity (CA). The CA of pure and doped GQDs was examined in the presence of a reducing agent ($NaBH_4$) and an oxidizing agent, rhodamine B (RhB), for the degradation of RhB. Freshly prepared 1.5 mL of RhB solution was added to the quartz cuvette containing 400 μL of prepared 0.1 M $NaBH_4$. Moreover, 400 μL of the prepared sample was dissolved into the solution. In the presence of $NaBH_4$, RhB was reduced to leuco RhB (LRhB), confirming the dye degradation. The following equation calculated degradation efficiency: degradation (%) $= (C_0 - C_t)/C_0 \times 100\%$, where C_0 and C_t are the initial and final concentrations of RhB.

2.2.2 Catalysis mechanism. The mechanism for the catalytic degradation of RhB involves the redox reaction between $NaBH_4$ and RhB. Initially, reactants adsorbed onto the surface of nano-material, $NaBH_4$ dissociates into BH_4^- and H^+ ions which RhB accepts, favoring the breakdown of organic dye. However, in the presence of $NaBH_4$ reaction was slow; to accelerate the degradation rate, synthesized specimens were added as catalysts. The enhanced catalytic rate was related to the significant interaction among the nucleophilic reducing agent and electrophilic dye on the large surface area of quantum dots. The catalyst functions as an electron relay, permitting the transfer of electrons and detached H atoms from BH_4^- to the cationic dye that results in the breakage of the double bond by π conjugation. Finally, pink RhB was reduced to colorless LRhB,[32,33] as shown in Fig. 2.

2.3 Biological activity

2.3.1 Sample collection. Direct milking into sterile glassware collected raw milk samples from lactating cows marketed at various markets, veterinary facilities, and farms in Punjab, Pakistan. Milk samples were brought to the lab after being acquired at 4 °C. Gram-negative (G −ve) *E. coli* bacteria found in raw milk were counted on MacConkey agar (MA). Cultured specimens were incubated for 48 h at 37 °C.

2.3.2 Identification and characterization of bacterial isolates. Using Bergey's Manual of Determinative Bacteriology as a reference, different biochemical and morphological strategies as gram staining based on colony morphology were applied to identify *E. coli* bacteria.[34]

2.3.2.1 Antibiotic susceptibility. On Mueller Hinton agar (MHA), the Bauer *et al.*[35] disk diffusion method was employed to conduct the antibiotic susceptibility test. The test was conducted to analyze whether the *E. coli* was resistant to the following antibiotics (classes); ceftriaxone (Cro) 30×10^{-6} g (cephalosporins), gentamicin (Gm) 10 μg (aminoglycosides), ciprofloxacin (Cip) 5×10^{-6} g (Quinolones), tetracycline (Te) 30×10^{-6} g (tetracyclines), imipenem (Imi) 10×10^{-6} g (carbapenem), amoxycillin (A) 30×10^{-6} g (penicillins), and azithromycin (Azm) 15×10^{-6} g (macrolides).[36] *E. coli* purified

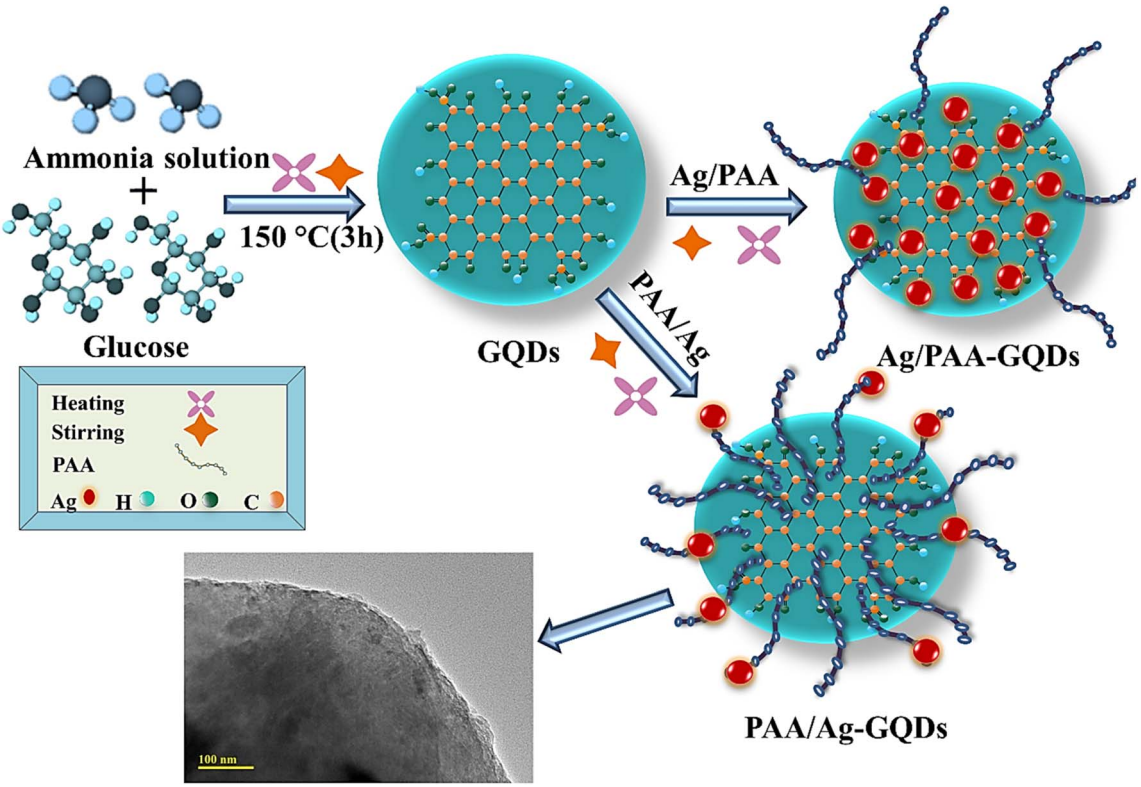

Fig. 1 Schematic synthesis of GQDs, Ag/PAA-GQDs and PAA/Ag-GQDs.

cultures were cultivated, and turbidity was brought to 0.5 MacFarland. After that, it was spread-plated on Muller Hinton Agar (MHA) (Oxoid Limited, Basingstoke, UK), and antibiotic disks were positioned apart from the inoculated infected plate's surface to preclude the overlap of inhibitory zones. Clinical and Laboratory Standard Institute was utilized to explain the results after the incubation of plates for 24 h at 37 °C.[37] Bacterium was proclaimed MDR if shown to resist at least three drugs.[38]

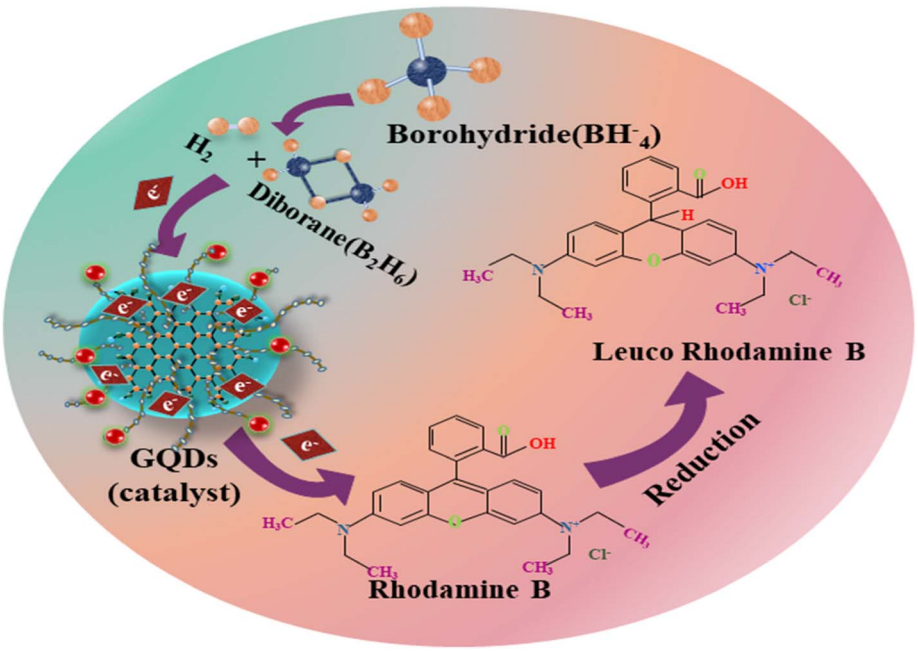

Fig. 2 Schematic diagram of the catalysis mechanism of GQDs, Ag/PAA-GQDs, and PAA/Ag-GQDs.

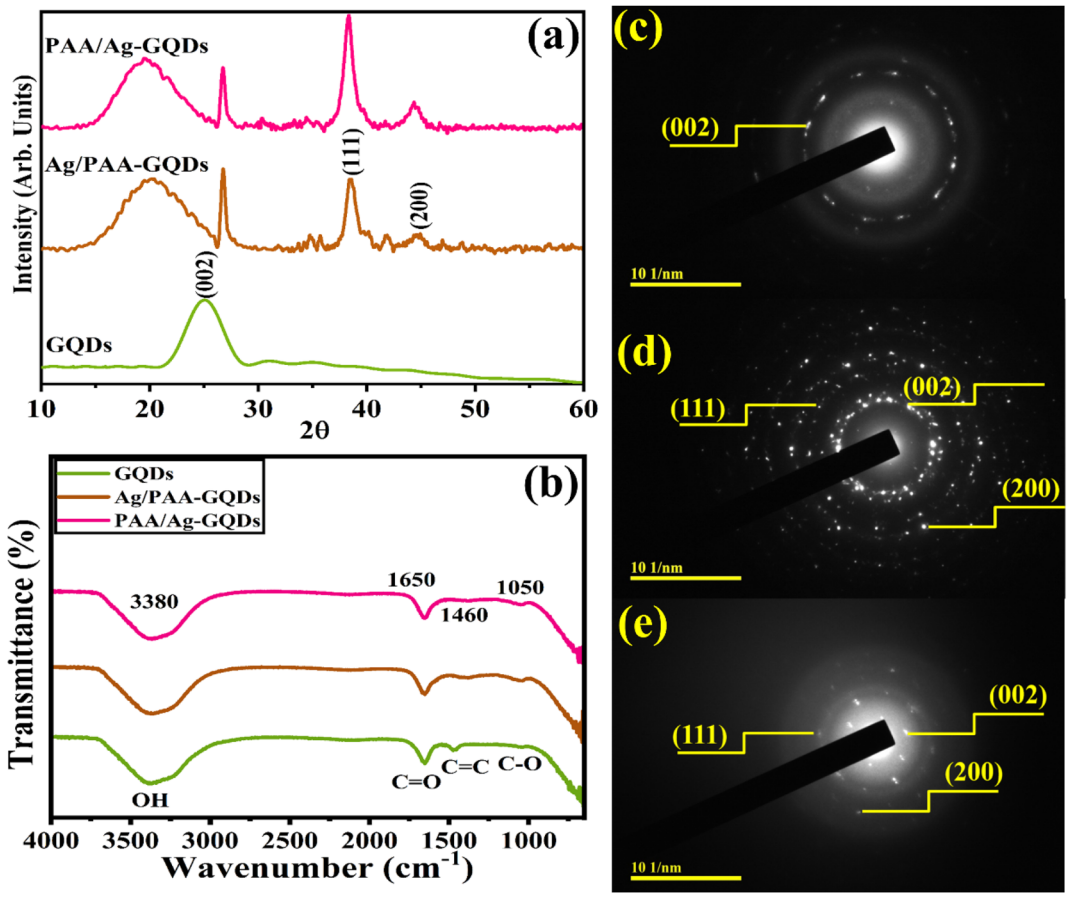

Fig. 3 (a) XRD patterns, (b) FTIR spectra, (c–e) SAED images of Ag/PAA-GQDs and PAA/Ag-GQDs.

2.3.2.2 Antimicrobial activity. Agar well diffusion procedure was employed to assay the *in vitro* antimicrobial potential of pure and doped GQDs upon ten isolates of MDR *E. coli* collected from mastitic milk by swabbing 1.5×10^8 CFU mL^{-1} (0.5 McFarland standard) MDR *E. coli* on MA. A sterile cork bore was used to bore well on MA plates having a diameter of 6 mm. Each well was filled with distinct concentrations as (0.5 mg/50 μL) and (1.0 mg/50 μL) of prepared samples by micropipette in contrast to ciprofloxacin (0.005 mg μL^{-1}) and deionized water (50 μL) referred as a positive and negative control, respectively.[39]

2.3.2.3 Statistical analysis. The inhibition zone in millimeters (mm) and inhibition zone diameters were determined by one-way analysis of variance (ANOVA) utilizing SPSS 20 for estimating the antimicrobial efficacy.[40]

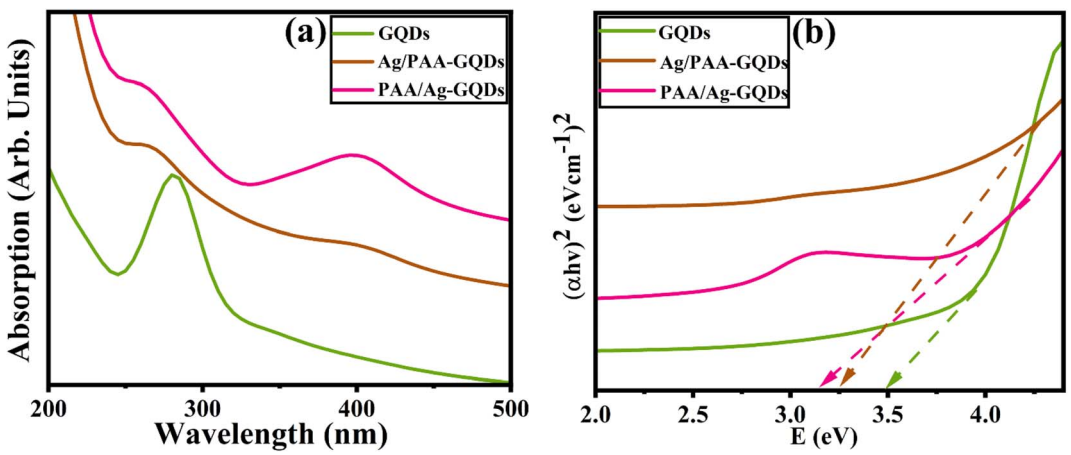

Fig. 4 (a) UV-visible spectra, (b) band gap energies of GQDs, Ag/PAA-GQDs, and PAA/Ag-GQDs.

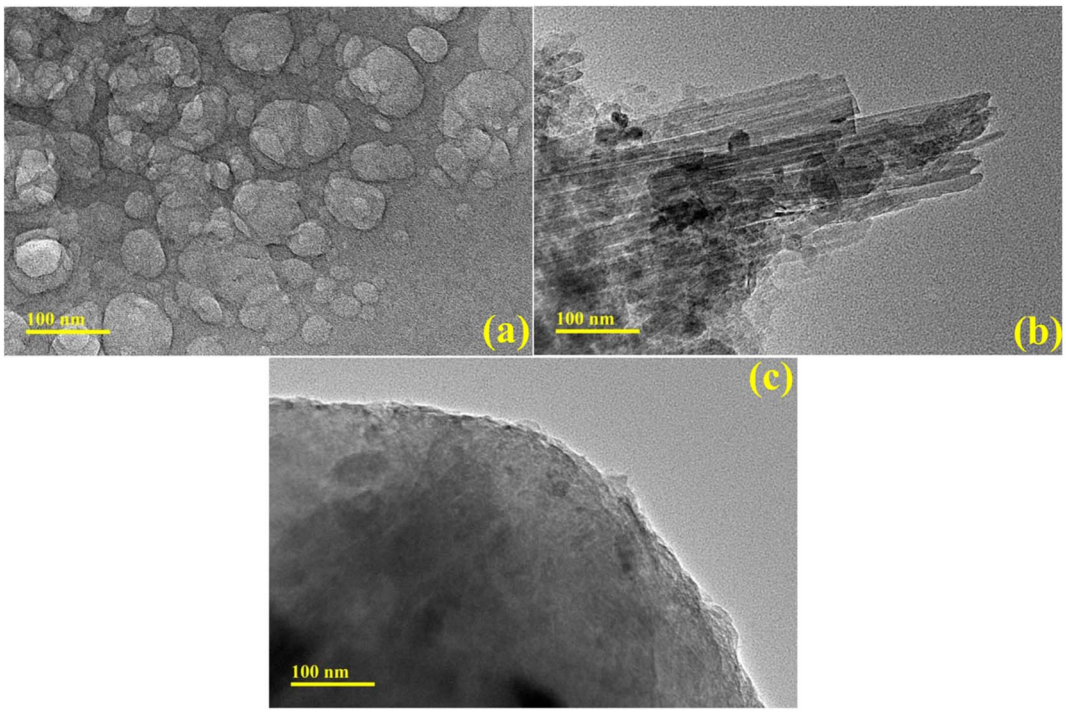

Fig. 5 TEM analysis of (a) GQDs, (b) Ag/PAA-GQDs, and (c) PAA/Ag-GQDs samples.

2.4 Molecular docking analysis

The cell wall production process disruption has been suggested as an attractive target for antibiotic research and as a possible mechanism behind the bactericidal action of different nanostructures. Enzymes pertaining to peptidoglycan production have enormous significance for the identification of novel antibacterial drugs since their inhibition results in the destruction of the cell wall and, eventually, the death of bacteria.[41,42] Similarly, enzymes pertaining to nucleic

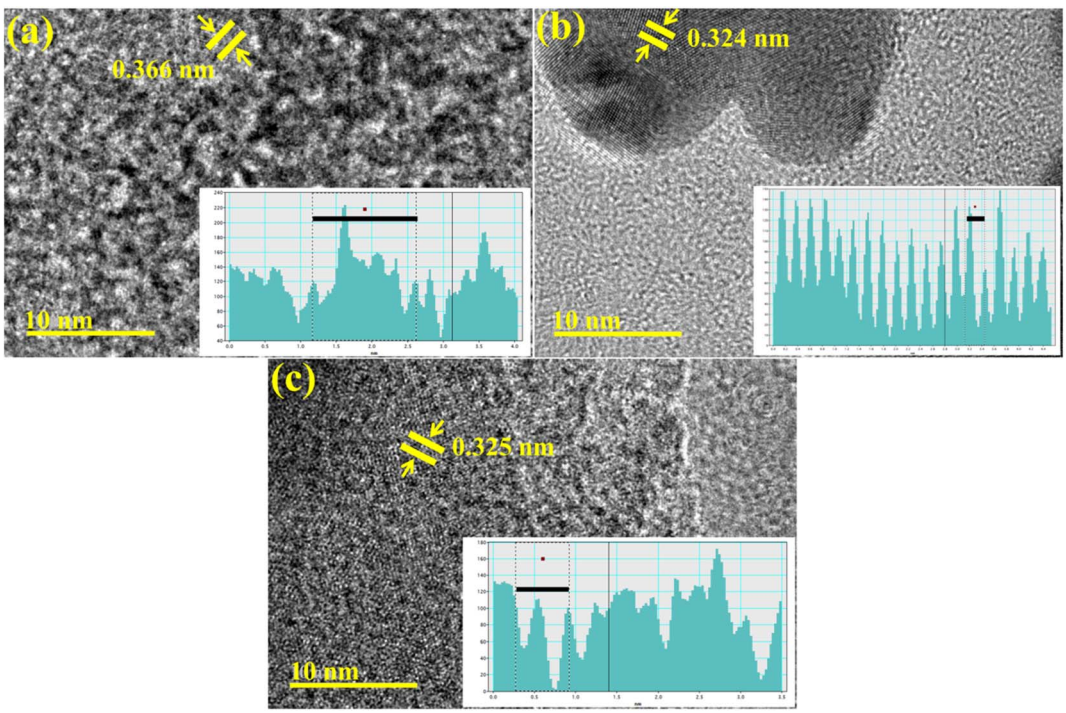

Fig. 6 HR-TEM micrographs of synthesized (a) GQDs, (b) Ag/PAA-GQDs, and (c) PAA/Ag-GQDs.

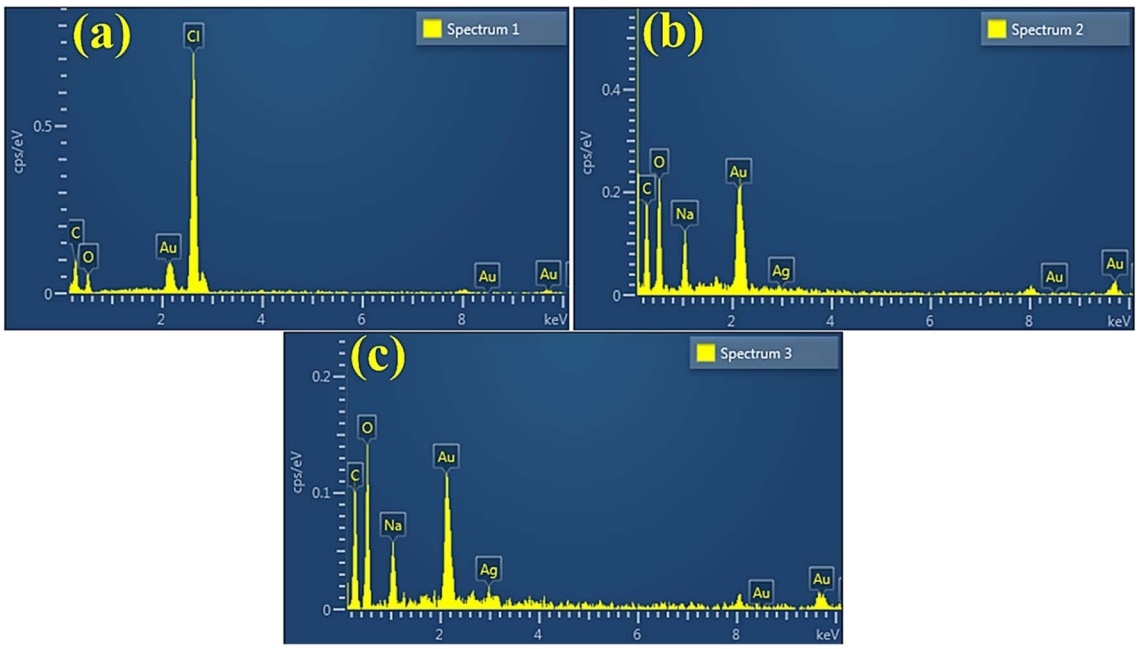

Fig. 7 EDS analysis of (a) GQDs (b) Ag/PAA-GQDs (c) PAA/Ag-GQDs.

acid biosynthesis, particularly DNA gyrase, have a significant impact on the identification of antibiotics.[43] Here, we evaluated the inhibitory ability of silver and polyacrylic acid-doped graphene quantum dots against β-lactamase and DNA gyrase enzymes from *E. coli*. Crystal structures of β-lactamase and DNA gyrase from *E. coli* were acquired from RCSB PDB (**https://www.rcsb.org**) with PDB codes 4KZ9 (resolution: 1.72)[44] and 5MMN (resolution: 1.90).[45] The docking investigation was executed using the SYBYL-X 2.0 program, as described in our previous studies.[46,47] The 3D structures of the chosen compounds were generated using the Sybyl-X2.0/SKETCH module (Fig. S1†). Subsequently, energy reduction was performed using the Tripos force field, using Gasteiger Hückel atomic charges. The Surflex-Dock module, a component of the SYBYL-X 2.0 molecular modelling software program, was used to conduct flexible molecular docking simulations. These simulations aimed to investigate the binding interactions between nanoparticles and the active site residues of certain proteins. Hydrogen atoms were inadvertently omitted. The allocation of atomic types and application of atomic charges were carried out in accordance with the AMBER 7 FF99 force field. Ultimately, by using the Powell method with a convergence gradient of 0.5 kcal (mol^{-1} A^{-1}) over a span of 1000 cycles, the energy was successfully reduced in order to mitigate steric conflicts. In order to ensure accuracy and reliability, a minimum of 20 optimal docked conformations were definitively preserved for each ligand–receptor complex system. The Hammerhead scoring system was used for the evaluation of the most favorable putative ligand conformations. The Surflex dock module employs an empirically derived consensus scoring function called cScore to generate and prioritize hypothetical orientations of ligand fragments.

3. Results and discussion

3.1 Characterization of catalyst

The crystalline phase purity and structural information of synthesized samples were assessed through XRD ranging from 10° to 60° (Fig. 3a). XRD peak of GQDs at 25.2° corresponds to the (002) plane.[48] Upon Ag/PAA doping, two distinct peaks were observed at 38.2° and 44.4° for (111) and (200) planes of cubic crystal structure (JCPDS No. 01-087-0718). Peaks shift towards a higher 2θ value upon incorporating Ag, confirmed interstitial site of Ag.[49] Furthermore, a broad diffraction peak observed at 18.7° corresponds to PAA and shows its amorphous nature.[50] FTIR Spectroscopy was utilized to determine the nature of surface functional groups. The transmittance band at 3380 cm^{-1} was ascribed to the stretching vibration of the hydroxyl (–OH) group.[51] The vibration band at 1460 cm^{-1} is assigned to the vibration of –C=C bonds of the aromatic system.[52,53] The band of the –C=O group (stretching mode) was centered at around 1650 cm^{-1}, evidenced by the edges functionality of the –C=O group.[52,54,55] The week –C–O stretching peak was also observed at ~1050 cm^{-1}.[56] Incorporating Ag and PAA into prepared GQDs indicated that one of the bands was shifted with decreased intensity due to metal–polymer interactions[57] (Fig. 3b). The selected area diffraction (SAED) pattern of GQDs, Ag/PAA-GQDs, and PAA/Ag-GQDs NSs showed bright rings associated with distinct XRD planes (002), (111), and (200) (Fig. 3c–e).

UV-VIS spectroscopy was utilized to analyze the optical properties of synthesized samples. GQDs showed absorption in the range of ~260–320 nm,[58] and a strong absorption peak was observed at ~280 nm, attributed to π–π* electronic transition of graphitic C=C domains in sp^2 cluster[59,60] as elaborated in (Fig. 4a). Tauc plot was used to calculate the band gap energy

(E_g) of GQDs as 3.5 eV, consistent with previously published data.[61,62] E_g of GQDs in the presence of capping was decreased from 3.5 to 3.10 and 3.2 eV. Upon doping, E_g values are the consequence of the enhanced quantum confinement effect with a decrease in domain size in GQDs[63] (Fig. 4b).

TEM analysis was performed to examine synthesized products' morphology and structural properties. TEM images of the control sample revealed the formation of quantum dots and, upon doping of Ag-PAA nanorods of Ag, occupied the surface of GQDs. Incorporating PAA-Ag in GQDs demonstrated an aggregation (Fig. 5a–c).

Additionally, the interlayer distance of GQDs, Ag/PAA-GQDs, and PAA/Ag-GQDs was calculated from HR-TEM micrographs using Gatan software as (0.366 nm, 0.324 nm, 0.325 nm) (Fig. 6a–c).

EDS spectra revealed carbon and oxygen peaks which confirmed the presence of GQDs. The prominent oxygen peak in doped samples generated from PAA, chemical formula $(C_3H_4O_2)_n$.[64] The chloride (Cl) and sodium (Na) peaks ascribed to HCl and NaOH were used in the synthesis to sustain the pH. The Ag peak confirmed the existence of Ag in doped samples, while small Au peaks attributed to the coating on the samples minimized charging effects[52,65] (Fig. 7a–c). Moreover, EDS mapping of the synthesized doped specimen was utilized to analyze its elemental constituent distribution pattern to check additional interfacial contact (Fig. 8a–c). Two components (Cu and O) were found to spread in doped samples. As mentioned, O, Cu, and Zn were assigned to contamination, the sample holder used for EDS analysis.

3.2 Catalytic properties of GQDs, Ag/PAA-GQDs, and PAA/Ag-GQDs

A UV-Vis spectrophotometer (200–800 nm) was used to assess the catalytic efficiency of Ag/PAA-GQDs and PAA/Ag-GQDs with $NaBH_4$ in acidic, basic, and neutral conditions. The spectroscopic results revealed the RhB degradation with some approximate errors (72.4 ± 0.8, 66.4 ± 0.9, 66.1 ± 1%) in neutral medium (pH = 7), (54. ± 1.3, 50.2 ± 2, 57.4 ± 2.3%) in basic medium (pH = 12) and (62.1 ± 1.1, 63.5 ± 1.8, 44.7 ± 2.2%) in acidic medium (pH = 4) illustrated in (Fig. 9a–c). The reduction of RhB occurred slowly (40 min) without a catalyst, which was calculated with some errors in acidic, basic, and neutral media, 25.2 ± 2.28, 21.8 ± 2.3, and 17.0 ± 1.2%, respectively (Fig. 9d). At pH = 7, the catalyst surface (GQDs) typically acquires a negative charge, which promotes the adsorption of positively charged RhB, thus accelerating the degradation rate. In an acidic medium, catalytic activity was increased, ascribed to the production of H^+ ions that adhere to the nano-material. In a basic medium, the concentration of hydroxyl ions increases, resulting in product oxidation and a significant reduction in catalytic performance. Upon doping of Ag/PAA, the degradation potential decreased as the Ag occupied active sites on a nano-

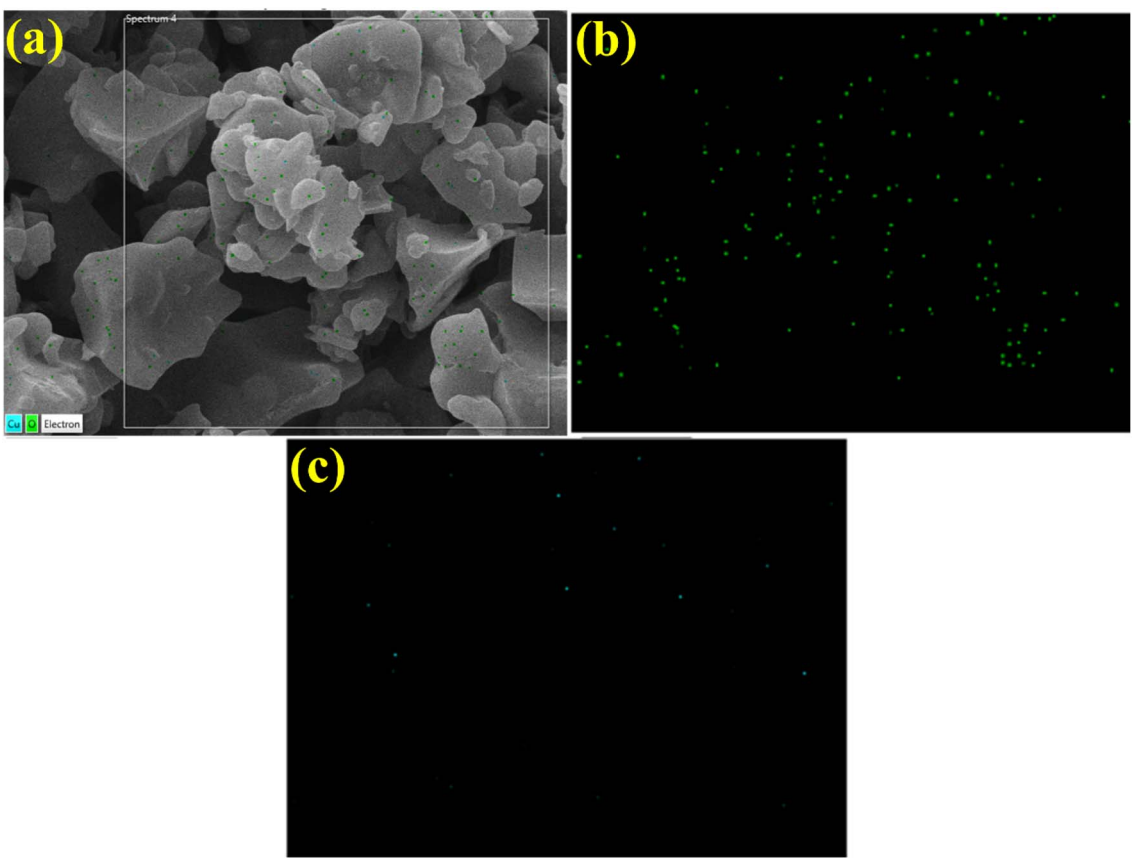

Fig. 8 EDS mapping of (a) GQDs (b) Ag/PAA-GQDs (c) PAA/Ag-GQDs.

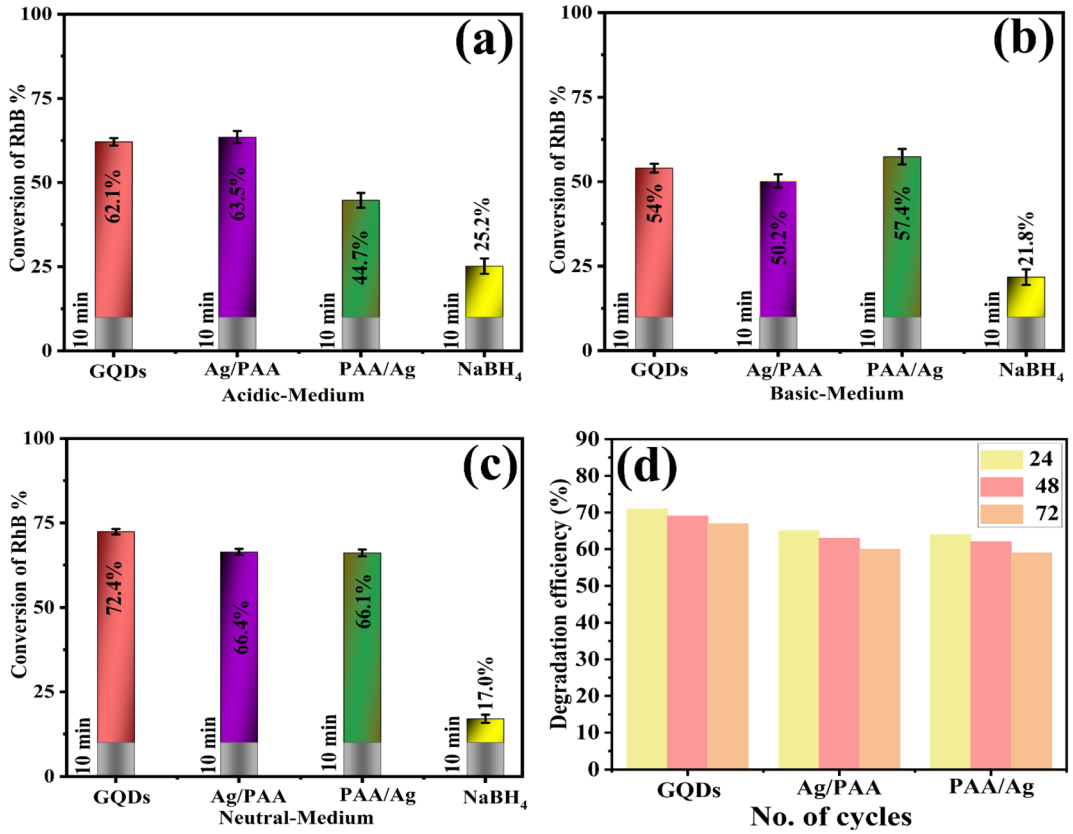

Fig. 9 Catalytic potential of GQDs, Ag/PAA-GQDs, and PAA/Ag-GQDs in (a) acidic, (b) basic, and (c) neutral media (d) catalysis recyclability studies.

material, reducing PAA adsorption. The incorporation of PAA/Ag in pure GQDs led to an increase in catalytic activity due to the presence of COOH, which exhibited electrostatic interactions with the catalyst.[66] The catalytic activity of pristine and doped GQDs is compared with the literature, as illustrated in Table 1.

3.3 Efficiency of GQDs, Ag/PAA-GQDs and PAA/Ag-GQDs

Moreover, the reusability of pure and doped GQDs catalysts was assessed by performing degradation using previously used samples. During each cycle, the catalyst was separated from the solution using centrifugation, washed with DI water, and heated overnight at 60 °C. The reusability of GQDs, Ag/PAA-GQDs, and PAA/Ag-GQDs were investigated over three consecutive cycles (24 h, 48 h, and 72 h) for the RhB degradation, as depicted in Fig. 9d.

X-ray photoelectron spectroscopy (XPS) was employed to characterize the spectrum of PAA/Ag-GQDs. The intent was to ascertain the elemental makeup and chemical nature of constituent elements. Fig S2a–d† exhibits the narrow range XPS spectra of generated samples, specifically highlighting the Ag O 1s and Ag 3d peaks. The measured binding strength of Ag O 1s in PAA/Ag-GQDs Fig. S2a† was determined to be 530.8 eV, therefore consistent with previous investigations.[72,73] The determination of the precise position of the binding strength spike was accomplished by considering the ionic and electronegativity characteristics of constituent atoms within the molecule. The findings are comparable with previous characterization techniques[74] and confirm that silver nanoparticles are

Table 1 Oxidation of RhB with H_2O_2 in the presence of different catalytic systems

Nano-materials	Catalyst concentration	RhB concentration	Conversion of RhB (%)	Ref.
Graphene quantum dots decorated titania nanosheets	2 mL	10.20 mg L^{-1}	56	67
Graphene quantum dots by P doping	100 mg	10 mg L^{-1}	58	68
Graphene quantum dot-based hydrogels	100 μg mL^{-1}	10 mg L^{-1}	62	69
Graphene quantum dots from corn powder	1 mg mL^{-1}	10 mg L^{-1}	45	70
Ag and polyacrylic acid (PAA) doped SrO	400 μL	3 mL	60.7	71
Silver and polyacrylic acid doped graphene quantum dots	400 μL	1.5 mL	66.4	Present work

Table 2 Antimicrobial efficacy of GQDs, Ag/PAA-GQDs and PAA/Ag-GQDs

Samples	Inhibition areas (mm) 0.5 mg/50 μL	Inhibition areas (mm) 1.0 mg/50 μL
GQDs	2.55	4.15
Ag/PAA-GQDs	3.15	5.25
PAA/Ag-GQDs	3.65	5.85
Ciprofloxacin	5.75	5.75
DI water	0	0

efficiently acquired following $NaBH_4$ reduction. On the contrary, the binding energies of 365.9 eV and 371.9 eV, accordingly, correspond to Ag $3d_{5/2}$ and Ag $3d_{3/2}$ Fig. S2b†.[75–78]

3.4 Biological activity

Antibacterial activity of doped and pure GQDs against *E. coli* was evaluated by agar well diffusion strategy. The inhibition zones were recorded as (4.15–5.85 mm) and (2.55–3.65 mm) at maximum and minimum doses, summarized in (Table 2). An inhibition region of 5.75 mm ciprofloxacin (positive control) and 0 nm of DI water (negative control) was calculated as illustrated in Fig S3a and b.† The inhibition diameter of pure GQDs was increased as the dopant was incorporated. Nanomaterial generated oxidative stress related to the crystallinity, surface area, and diffusion ability. Ag/PAA-GQDs exhibited superior antimicrobial performance because Ag provides a large surface area, producing more reactive oxygen species (ROS) that lead to cell necrosis. Carboxyl and the hydroxyl group of PAA increased the production of ROS, leading to the extrusion of cytoplasmic components that eventually caused bacterial death. Doped GQDs destroy the bacterial cell by membrane distortion, enzymes inactivation, proteins denaturation, leakage of cytoplasmic components and DNA deterioration, *etc.*,[66–68,79–81] as displayed (Fig. S4†).

In the past few decades, there has been significant interest in molecular docking predictions for deciphering the enigma behind many biological functions. The significance of cell wall synthesis (*i.e.*, peptidoglycan production) and the nucleic acid biosynthetic route for identifying antibiotics is well established.[82,83] In spite of the fact that the antibacterial activity of several nanostructures has been described in recent years,[84,85] the specific mechanism of their actions requires additional investigation. The silver and polyacrylic acid-doped graphene quantum dots had a high binding score (5.13) inside the binding pocket of the β-lactamase enzyme in *E. coli*. The binding interaction pattern with important amino acid residues is shown in (Fig. 10a–c) *via* H-bonding with Gln120 and Asn152. The molecular docking predictions of silver and polyacrylic acid doped graphene quantum dots against DNA gyrase of *E. coli* revealed H-bonds with key amino acid residues such as Arg76, Thr165, and Gly77 (shown in Fig. 10d–f).

The binding tendency of silver and polyacrylic acid doped graphene quantum dots revealed through molecular docking predicted these NPs as potential inhibitors of β-lactamase and DNA gyrase enzyme that is suggested to be further confirmed by *in vitro* enzyme inhibition techniques.

4. Summary

In this research work, GQDs, Ag/PAA-doped GQDs and PAA/Ag-doped GQDs were successfully synthesized by the cost-effective carbonization method to remove various organic and inorganic hazardous pollutants. XRD diffraction peak of the GQDs is centered at 25.2° corresponding to the (002) plane with a *d*-

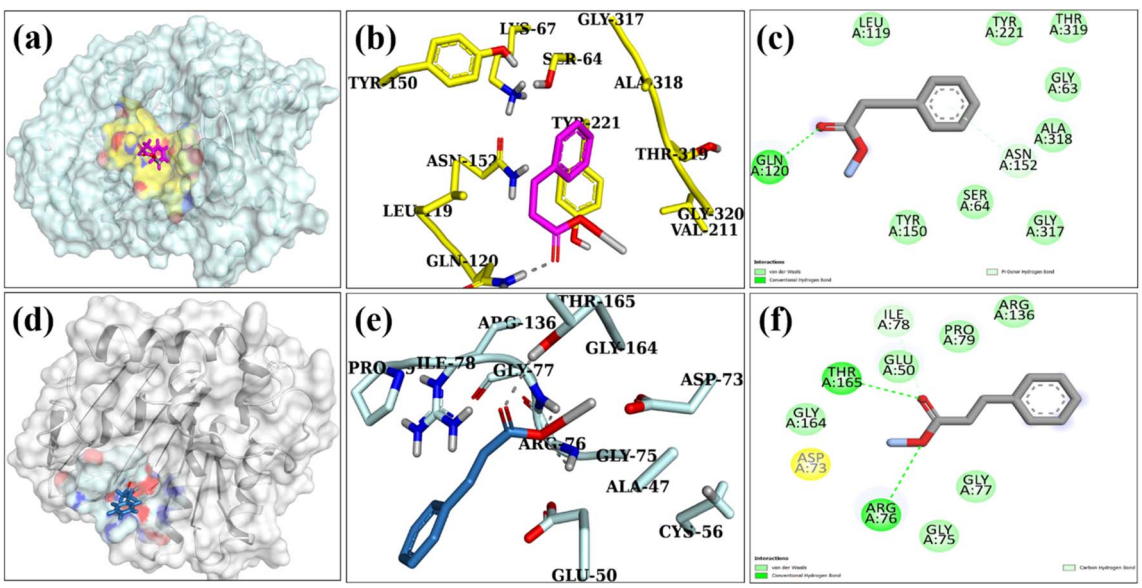

Fig. 10 Binding interaction pattern with active site residues of β-lactamase (a–c) and DNA gyrase (d–f) enzyme from *E. coli* where (a and d) represents binding pocket, (b and e) 3D structure and (c and f) 2D structure of NPs in the active site of selected proteins.

spacing of 0.366 nm. The increase in E_g from 3.03 to 3.14 eV accompanied by blue shift was exposed by UV-Vis spectroscopy. FTIR confirmed the presence of GQDs by displaying the vibration band of the sp^2 carbon plane. TEM results confirmed that Ag particles attached to the surface of GQDs and PAA formed a layer on the surface of GQDs additionally, HRTEM micrographs revealed interlayer *d*-spacing (0.366 nm, 0.324 nm, 0.325 nm). EDS spectra revealed the presence of C, O, Au, and Ag, confirming the elemental composition of pristine and doped GQDs. The maximum RhB deterioration rate of 57.42% and 66.41% in basic and neutral media was observed for pure and PAA/Ag-GQDs, respectively. *In silico* docking studies identified inhibition of β-lactamase and DNA gyrase as potential mechanisms underlying silver and polyacrylic acid doped graphene quantum dots bactericidal behavior. Furthermore, the significant inhabitation zone (5.85 mm) of PAA/Ag-GQDs against *E. coli* was recorded. In conclusion, these findings imply that synthesized pure and doped GQDs effectively eliminate toxic effluents from industrial wastewater (dye degradation) and are effective against pathogens, low cost, environment-friendly, and can be used in the future.

Conflicts of interest

The authors declare "no conflict of interest".

Acknowledgements

The authors extend their appreciation to the Deanship of Scientific Research at King Khalid University, Saudi Arabia for funding this work through Large Groups Project under Grant Number (RGP.1/248/44).

References

1 S. Shukla and A. Saxena, Groundwater quality and associated human health risk assessment in parts of Raebareli district, Uttar Pradesh, India, *Groundwater for Sustainable Development*, 2020, vol. 10, p. 100366.
2 S. Imtiazuddin, M. Mumtaz and K. A. Mallick, Pollutants of wastewater characteristics in textile industries, *J. Basic Appl. Sci.*, 2012, **8**, 554–556.
3 M. Zienkiewicz-Strzałka, A. Deryło-Marczewska and R. B. Kozakevych, Silica nanocomposites based on silver nanoparticles-functionalization and pH effect, *Appl. Nanosci.*, 2018, **8**(7), 1649–1668.
4 S. Chowdhury and P. Saha, Adsorption kinetic modeling of safranin onto rice husk biomatrix using pseudo-first-and pseudo-second-order kinetic models: Comparison of linear and non-linear methods, *Clean: Soil, Air, Water*, 2011, **39**(3), 274–282.
5 R. Jain, M. Mathur, S. Sikarwar and A. Mittal, Removal of the hazardous dye rhodamine B through photocatalytic and adsorption treatments, *J. Environ. Manage.*, 2007, **85**(4), 956–964.
6 J. Lonnen, S. Kilvington, S. C. Kehoe, F. Al-Touati and K. G. McGuigan, Solar and photocatalytic disinfection of protozoan, fungal and bacterial microbes in drinking water, *Water Res.*, 2005, **39**(5), 877–883.
7 S. Moniri Javadhesari, S. Alipour, S. Mohammadnejad and M. R. Akbarpour, Antibacterial activity of ultra-small copper oxide (II) nanoparticles synthesized by mechanochemical processing against S. aureus and E. coli, *Mater. Sci. Eng., C*, 2019, **105**, 110011.
8 M. Kosek, C. Bern and R. L. Guerrant, The global burden of diarrhoeal disease, as estimated from studies published between 1992 and 2000, *Bull. W. H. O.*, 2003, **81**, 197–204.
9 S. Rengaraj, K.-H. Yeon and S.-H. Moon, Removal of chromium from water and wastewater by ion exchange resins, *J. Hazard. Mater.*, 2001, **87**(1), 273–287.
10 A. W. Zularisam, A. F. Ismail and R. Salim, Behaviours of natural organic matter in membrane filtration for surface water treatment — a review, *Desalination*, 2006, **194**(1), 211–231.
11 M.-X. Zhu, L. Lee, H.-H. Wang and Z. Wang, Removal of an anionic dye by adsorption/precipitation processes using alkaline white mud, *J. Hazard. Mater.*, 2007, **149**(3), 735–741.
12 G. Centi, P. Ciambelli, S. Perathoner and P. Russo, Environmental catalysis: trends and outlook, *Catal. Today*, 2002, **75**(1), 3–15.
13 T.-Y. Shin, S.-H. Yoo and S. Park, Gold nanotubes with a nanoporous wall: their ultrathin platinum coating and superior electrocatalytic activity toward methanol oxidation, *Chem. Mater.*, 2008, **20**(17), 5682–5686.
14 Y. Xian, F. Gao and B. Cai, Synthesis of platinum nanoparticle chains based on α-chymotrpsin fibrils, *Mater. Lett.*, 2013, **111**, 39–42.
15 J. Ge, T. Huynh, Y. Hu and Y. Yin, Hierarchical magnetite/silica nanoassemblies as magnetically recoverable catalyst–supports, *Nano Lett.*, 2008, **8**(3), 931–934.
16 F. Liu, J. Yang, J. Zuo, D. Ma, L. Gan, B. Xie, P. Wang and B. Yang, Graphene-supported nanoscale zero-valent iron: Removal of phosphorus from aqueous solution and mechanistic study, *J. Environ. Sci.*, 2014, **26**(8), 1751–1762.
17 R. S. Kalhapure, S. J. Sonawane, D. R. Sikwal, M. Jadhav, S. Rambharose, C. Mocktar and T. Govender, Solid lipid nanoparticles of clotrimazole silver complex: An efficient nano antibacterial against Staphylococcus aureus and MRSA, *Colloids Surf., B*, 2015, **136**, 651–658.
18 S. Lekamge, A. S. Ball, R. Shukla and D. Nugegoda, The toxicity of nanoparticles to organisms in freshwater, *Rev. Environ. Contam. Toxicol.*, 2020, **248**, 1–80.
19 S. Kumar, R. Sharma, V. Sharma, G. Harith, V. Sivakumar and V. Krishnan, Role of RGO support and irradiation source on the photocatalytic activity of CdS–ZnO semiconductor nanostructures, *Beilstein J. Nanotechnol.*, 2016, **7**(1), 1684–1697.
20 A. Kumar and G. Pandey, A review on the factors affecting the photocatalytic degradation of hazardous materials, *Mater. Sci. Eng. Int. J.*, 2017, **1**(3), 1–10.
21 X. Wang, L. Zhi and K. Müllen, Transparent, conductive graphene electrodes for dye-sensitized solar cells, *Nano Lett.*, 2008, **8**(1), 323–327.

22 S.-M. Paek, E. Yoo and I. Honma, Enhanced cyclic performance and lithium storage capacity of SnO2/graphene nanoporous electrodes with three-dimensionally delaminated flexible structure, *Nano Lett.*, 2009, **9**(1), 72–75.
23 L. A. Ponomarenko, F. Schedin, M. I. Katsnelson, R. Yang, E. W. Hill, K. S. Novoselov and A. K. Geim, Chaotic Dirac billiard in graphene quantum dots, *Science*, 2008, **320**(5874), 356–358.
24 X. Yan, X. Cui, B. Li and L.-s. Li, Large, solution-processable graphene quantum dots as light absorbers for photovoltaics, *Nano Lett.*, 2010, **10**(5), 1869–1873.
25 E. Lee, J. Ryu and J. Jang, Fabrication of graphene quantum dots via size-selective precipitation and their application in upconversion-based DSSCs, *Chem. Commun.*, 2013, **49**(85), 9995–9997.
26 X. Wang, L. Cao, F. Lu, M. J. Meziani, H. Li, G. Qi, B. Zhou, B. A. Harruff, F. Kermarrec and Y.-P. Sun, Photoinduced electron transfers with carbon dots, *Chem. Commun.*, 2009, (25), 3774–3776.
27 L. Li, G. Wu, G. Yang, J. Peng, J. Zhao and J.-J. Zhu, Focusing on luminescent graphene quantum dots: current status and future perspectives, *Nanoscale*, 2013, **5**(10), 4015–4039.
28 M. R. Shaik, M. Kuniyil, M. Khan, N. Ahmad, A. Al-Warthan, M. R. H. Siddiqui and S. F. Adil, Modified polyacrylic acid-zinc composites: synthesis, characterization and biological activity, *Molecules*, 2016, **21**(3), 292.
29 M. Mavaei, A. Chahardoli, Y. Shokoohinia, A. Khoshroo and A. Fattahi, One-step Synthesized Silver Nanoparticles Using Isoimperatorin: Evaluation of Photocatalytic, and Electrochemical Activities, *Sci. Rep.*, 2020, **10**(1), 1762.
30 S. Iqbal, M. Javed, A. Bahadur, M. A. Qamar, M. Ahmad, M. Shoaib, M. Raheel, N. Ahmad, M. B. Akbar and H. Li, Controlled synthesis of Ag-doped CuO nanoparticles as a core with poly(acrylic acid) microgel shell for efficient removal of methylene blue under visible light, *J. Mater. Sci.: Mater. Electron.*, 2020, **31**(11), 8423–8435.
31 X. T. Zheng, A. Than, A. Ananthanaraya, D.-H. Kim and P. Chen, Graphene quantum dots as universal fluorophores and their use in revealing regulated trafficking of insulin receptors in adipocytes, *ACS Nano*, 2013, **7**(7), 6278–6286.
32 S. A. Bhat, N. Rashid, M. A. Rather, S. A. Bhat, P. P. Ingole and M. A. Bhat, Highly efficient catalytic reductive degradation of Rhodamine-B over Palladium-reduced graphene oxide nanocomposite, *Chem. Phys. Lett.*, 2020, **754**, 137724.
33 P. Nagajyoyhi, K. Devarayapalli, T. Sreekanth, S. P. Vattikuti and J. Shim, Effective catalytic degradation of rhodamine B using ZnCO2O4 nanodice, *Mater. Res. Express*, 2019, **6**(10), 105069.
34 C. G. Sinclair, Bergey's Manual of Determinative Bacteriology, *Am. J. Trop. Med. Hyg.*, 1939, **1**(6), 605–606.
35 A. Bauer, Antibiotic susceptibility testing by a standardized single diffusion method, *Am. J. Clin. Pathol.*, 1966, **45**, 493–496.
36 F. Adzitey, S. Yussif, R. Ayamga, S. Zuberu, F. Addy, G. Adu-Bonsu, N. Huda and R. Kobun, Antimicrobial Susceptibility and Molecular Characterization of Escherichia coli Recovered from Milk and Related Samples, *Microorganisms*, 2022, **10**(7), 1335.
37 I. Lewis and S. James, *Performance standards for antimicrobial susceptibility testing*, 2022.
38 B. Iwalokun, A. Ogunledun, D. Ogbolu, S. Bamiro and J. Jimi-Omojola, In vitro antimicrobial properties of aqueous garlic extract against multidrug-resistant bacteria and Candida species from Nigeria, *J. Med. Food*, 2004, **7**(3), 327–333.
39 A. Haider, M. Ijaz, M. Imran, M. Naz, H. Majeed, J. A. Khan, M. M. Ali and M. Ikram, Enhanced bactericidal action and dye degradation of spicy roots' extract-incorporated fine-tuned metal oxide nanoparticles, *Appl. Nanosci.*, 2020, **10**(4), 1095–1104.
40 A. Haider, M. Ijaz, S. Ali, J. Haider, M. Imran, H. Majeed, I. Shahzadi, M. M. Ali, J. A. Khan and M. Ikram, Green Synthesized Phytochemically (Zingiber officinale and Allium sativum) Reduced Nickel Oxide Nanoparticles Confirmed Bactericidal and Catalytic Potential, *Nanoscale Res. Lett.*, 2020, **15**(1), 50.
41 J. Buxeraud and S. Faure, Les bêtalactamines, *Actual. Pharm.*, 2016, **55**(558), 1–5.
42 D. Lim and N. C. J. Strynadka, Structural basis for the β lactam resistance of PBP2a from methicillin-resistant Staphylococcus aureus, *Nat. Struct. Biol.*, 2002, **9**(11), 870–876.
43 M. M. Mullis, I. M. Rambo, B. J. Baker and B. K. Reese, Diversity, ecology, and prevalence of antimicrobials in nature, *Front. Microbiol.*, 2019, 2518.
44 S. Barelier, O. Eidam, I. Fish, J. Hollander, F. Figaroa, R. Nachane, J. J. Irwin, B. K. Shoichet and G. Siegal, Increasing chemical space coverage by combining empirical and computational fragment screens, *ACS Chem. Biol.*, 2014, **9**(7), 1528–1535.
45 P. Panchaud, T. Bruyere, A.-C. Blumstein, D. Bur, A. Chambovey, E. A. Ertel, M. Gude, C. Hubschwerlen, L. Jacob and T. Kimmerlin, Discovery and optimization of isoquinoline ethyl ureas as antibacterial agents, *J. Med. Chem.*, 2017, **60**(9), 3755–3775.
46 I. Shahzadi, M. Islam, H. Saeed, A. Haider, A. Shahzadi, J. Haider, N. Ahmed, A. Ul-Hamid, W. Nabgan, M. Ikram and H. A. Rathore, Formation of biocompatible MgO/cellulose grafted hydrogel for efficient bactericidal and controlled release of doxorubicin, *Int. J. Biol. Macromol.*, 2022, **220**, 1277–1286.
47 M. Ikram, K. Chaudhary, A. Shahzadi, A. Haider, I. Shahzadi, A. Ul-Hamid, N. Abid, J. Haider, W. Nabgan and A. R. Butt, Chitosan/starch-doped MnO2 nanocomposite served as dye degradation, bacterial activity, and insilico molecular docking study, *Mater. Today Nano*, 2022, **20**, 100271.
48 A. K. Chaturvedi, A. Pappu and M. K. Gupta, Unraveling the role of agro waste-derived graphene quantum dots on dielectric and mechanical property of the fly ash based polymer nanocomposite, *J. Alloys Compd.*, 2022, **903**, 163953.
49 B. D. Ahn, H. S. Kang, J. H. Kim, G. H. Kim, H. W. Chang and S. Y. Lee, Synthesis and analysis of Ag-doped ZnO, *J. Appl. Phys.*, 2006, **100**(9), 093701.

50 S. K. Swain and K. Prusty, Biomedical applications of acrylic-based nanohydrogels, *J. Mater. Sci.*, 2018, **53**(4), 2303–2325.
51 M. Zain Ul Abidin, M. Ikram, A. Haider, A. Ul-Hamid, W. Nabgan, M. Imran, S. Goumri-Said and M. Benali Kanoun, Catalytic degradation of methylene blue and bactericidal action by silver and CS-doped iron oxide nanostructures: Experimental and DFT approaches, *Mater. Chem. Phys.*, 2023, **308**, 128300.
52 T. T. B. Quyen, N. H. Nhon, T. N. T. Duong, N. N. T. My, D. V. H. Thien and L. H. V. Thanh, Rapid and Simple Synthesis of Graphene Quantum dots/Ag Nanocomposites and Its Application for Glucose Detection by Photoluminescence Spectroscopy, *Int. J. Sci. Eng. Sci.*, 2021, **5**(6), 1–5.
53 T. Fan, W. Zeng, W. Tang, C. Yuan, S. Tong, K. Cai, Y. Liu, W. Huang, Y. Min and A. J. Epstein, Controllable size-selective method to prepare graphene quantum dots from graphene oxide, *Nanoscale Res. Lett.*, 2015, **10**(1), 55.
54 M. Roushani, M. Mavaei and H. R. Rajabi, Graphene quantum dots as novel and green nano-materials for the visible-light-driven photocatalytic degradation of cationic dye, *J. Mol. Catal. A: Chem.*, 2015, **409**, 102–109.
55 R. K. Biroju, G. Rajender and P. K. Giri, On the origin and tunability of blue and green photoluminescence from chemically derived graphene: Hydrogenation and oxygenation studies, *Carbon*, 2015, **95**, 228–238.
56 J. Zhang, M. S. Azam, C. Shi, J. Huang, B. Yan, Q. Liu and H. Zeng, Poly (acrylic acid) functionalized magnetic graphene oxide nanocomposite for removal of methylene blue, *RSC Adv.*, 2015, **5**(41), 32272–32282.
57 C.-C. Yang, S.-J. Lin and S.-T. Hsu, Synthesis and characterization of alkaline polyvinyl alcohol and poly(epichlorohydrin) blend polymer electrolytes and performance in electrochemical cells, *J. Power Sources*, 2003, **122**(2), 210–218.
58 S. Iravani and R. S. Varma, Green synthesis, biomedical and biotechnological applications of carbon and graphene quantum dots. A review, *Environ. Chem. Lett.*, 2020, **18**(3), 703–727.
59 M. Shehab, S. Ebrahim and M. Soliman, Graphene quantum dots prepared from glucose as optical sensor for glucose, *J. Lumin.*, 2017, **184**, 110–116.
60 G. Rajender and P. Giri, Formation mechanism of graphene quantum dots and their edge state conversion probed by photoluminescence and Raman spectroscopy, *J. Mater. Chem. C*, 2016, **4**(46), 10852–10865.
61 Y. Yan, J. Chen, N. Li, J. Tian, K. Li, J. Jiang, J. Liu, Q. Tian and P. Chen, Systematic bandgap engineering of graphene quantum dots and applications for photocatalytic water splitting and CO2 reduction, *ACS Nano*, 2018, **12**(4), 3523–3532.
62 H. S. Al Ghamdi and A. A. Al-Ghamdi, Opening band gap of multi-color graphene quantum dots using D-fructose as a green precursor, *Alexandria Eng. J.*, 2023, **79**, 155–163.
63 J. Peng, W. Gao, B. K. Gupta, Z. Liu, R. Romero-Aburto, L. Ge, L. Song, L. B. Alemany, X. Zhan and G. Gao, Graphene quantum dots derived from carbon fibers, *Nano Lett.*, 2012, **12**(2), 844–849.
64 T. Shujah, A. Shahzadi, A. Haider, M. Mustajab, A. M. Haider, A. Ul-Hamid, J. Haider, W. Nabgan and M. Ikram, Molybdenum-doped iron oxide nanostructures synthesized via a chemical co-precipitation route for efficient dye degradation and antimicrobial performance: in silico molecular docking studies, *RSC Adv.*, 2022, **12**(54), 35177–35191.
65 A. D. Khan, M. Ikram, A. Haider, A. Ul-Hamid, W. Nabgan and J. Haider, Polyvinylpyrrolidone and chitosan-doped lanthanum oxide nanostructures used as anti-bacterial agents and nano-catalyst, *Appl. Nanosci.*, 2022, **12**(7), 2227–2239.
66 F. Jamal, M. Ikram, A. Haider, A. Ul-Hamid, M. Ijaz, W. Nabgan, J. Haider and I. Shahzadi, Facile synthesis of silver and polyacrylic acid doped magnesium oxide nanostructure for photocatalytic dye degradation and bactericidal behavior, *Appl. Nanosci.*, 2022, **12**(8), 2409–2419.
67 S. Bian, C. Zhou, P. Li, J. Liu, X. Dong and F. Xi, Graphene Quantum Dots Decorated Titania Nanosheets Heterojunction: Efficient Charge Separation and Enhanced Visible-Light Photocatalytic Performance, *ChemCatChem*, 2017, **9**(17), 3349–3357.
68 J. Qian, C. Shen, J. Yan, F. Xi, X. Dong and J. Liu, Tailoring the Electronic Properties of Graphene Quantum Dots by P Doping and Their Enhanced Performance in Metal-Free Composite Photocatalyst, *J. Phys. Chem. C*, 2018, **122**(1), 349–358.
69 A. Ibarbia, L. Sánchez-Abella, L. Lezama, H. J. Grande and V. Ruiz, Graphene quantum dot-based hydrogels for photocatalytic degradation of organic dyes, *Appl. Surf. Sci.*, 2020, **527**, 146937.
70 H. Teymourinia, M. Salavati-Niasari, O. Amiri and H. Safardoust-Hojaghan, Synthesis of graphene quantum dots from corn powder and their application in reduce charge recombination and increase free charge carriers, *J. Mol. Liq.*, 2017, **242**, 447–455.
71 H. Shahzad, M. Imran, A. Haider, S. Naz, E. Umar, A. Ul-Hamid, W. Nabgan, M. M. Algaradah, A. M. Fouda, J. Haider and M. Ikram, Catalytic and antimicrobial properties of Ag and polyacrylic acid doped SrO nanocomposites; molecular docking analysis, *J. Photochem. Photobiol., A*, 2023, **444**, 114970.
72 Y. H. Kim, D. K. Lee, H. G. Cha, C. W. Kim and Y. S. Kang, Synthesis and Characterization of Antibacterial Ag−SiO2 Nanocomposite, *J. Phys. Chem. C*, 2007, **111**(9), 3629–3635.
73 Y. Sohn, SiO2 nanospheres modified by Ag nanoparticles: Surface charging and CO oxidation activity, *J. Mol. Catal. A: Chem.*, 2013, **379**, 59–67.
74 C. Gao, X. Wang, H. Wang, J. Zhou, S. Zhai and Q. An, Highly efficient and stable catalysis of p-nitrophenol via silver/lignin/polyacrylic acid hydrogel, *Int. J. Biol. Macromol.*, 2020, **144**, 947–953.
75 Y. Yan, J. Fu, M. Wang, S. Liu, Q. Xin, Z. Chen and Q. Xu, Fabrication of poly (cyclotriphosphazene-co-4, 4′-sulfonyldiphenol) nanotubes decorated with Ag–Au

bimetallic nanoparticles with enhanced catalytic activity for the reduction of 4-nitrophenol, *RSC Adv.*, 2016, **6**(30), 24921–24928.

76 D.-W. Cho, S. Kim, Y. F. Tsang and H. Song, Preparation of nitrogen-doped Cu-biochar and its application into catalytic reduction of p-nitrophenol, *Environ. Geochem. Health*, 2019, **41**(4), 1729–1737.

77 M. Bano, D. Ahirwar, M. Thomas, G. A. Naikoo, M. U.-D. Sheikh and F. Khan, Hierarchical synthesis of silver monoliths and their efficient catalytic activity for the reduction of 4-nitrophenol to 4-aminophenol, *New J. Chem.*, 2016, **40**(8), 6787–6795.

78 N. Muthuchamy, A. Gopalan and K.-P. Lee, A new facile strategy for higher loading of silver nanoparticles onto silica for efficient catalytic reduction of 4-nitrophenol, *RSC Adv.*, 2015, **5**(93), 76170–76181.

79 A. H. Jabbar, H. S. O. Al-janabi, M. Q. Hamzah, S. O. Mezan, A. N. Tumah, A. S. B. Ameruddin and M. A. Agam, Green synthesis and characterization of silver nanoparticle (AgNPs) using pandanus atrocarpus extract, *Int. J. Adv. Sci. Technol.*, 2020, **29**(3), 4913–4922.

80 Y. Cai, D. Wu, X. Zhu, W. Wang, F. Tan, J. Chen, X. Qiao and X. Qiu, Sol-gel preparation of Ag-doped MgO nanoparticles with high efficiency for bacterial inactivation, *Ceram. Int.*, 2017, **43**(1), 1066–1072.

81 A. Miškovská, M. Rabochová, J. Michailidu, J. Masák, A. Čejková, J. Lorinčík and O. Maťátková, Antibiofilm activity of silver nanoparticles biosynthesized using viticultural waste, *PLoS One*, 2022, **17**(8), e0272844.

82 S. Shaikh, J. Fatima, S. Shakil, S. M. D. Rizvi and M. A. Kamal, Antibiotic resistance and extended spectrum beta-lactamases: Types, epidemiology and treatment, *Saudi J. Biol. Sci.*, 2015, **22**(1), 90–101.

83 M. Díez-Aguilar, M. I. Morosini, A. P. Tedim, I. Rodríguez, Z. Aktaş and R. Cantón, Antimicrobial activity of fosfomycin-tobramycin combination against Pseudomonas aeruginosa isolates assessed by time-kill assays and mutant prevention concentrations, *Antimicrob. Agents Chemother.*, 2015, **59**(10), 6039–6045.

84 N. R. Bury and C. M. Wood, Mechanism of branchial apical silver uptake by rainbow trout is via the proton-coupled Na+ channel, *Am. J. Physiol.: Regul., Integr. Comp. Physiol.*, 1999, **277**(5), R1385–R1391.

85 A. Arsalan and H. Younus, Enzymes and nanoparticles: Modulation of enzymatic activity via nanoparticles, *Int. J. Biol. Macromol.*, 2018, **118**, 1833–1847.